Clinical Cancer Research

Functional Subclone Profiling for Prediction of Treatment-Induced Intratumor Population Shifts and Discovery of Rational Drug Combinations in Human Glioblastoma

Roman Reinartz[1,2], Shanshan Wang[3], Sied Kebir[1,2], Daniel J. Silver[4], Anja Wieland[1,2], Tong Zheng[3], Marius Küpper[1,2], Laurèl Rauschenbach[1,2], Rolf Fimmers[5], Timothy M. Shepherd[6], Daniel Trageser[1,2,7], Andreas Till[1,2], Niklas Schäfer[1,2], Martin Glas[1,2,7], Axel M. Hillmer[8], Sven Cichon[9], Amy A. Smith[10], Torsten Pietsch[11], Ying Liu[12], Brent A. Reynolds[3], Anthony Yachnis[13], David W. Pincus[3], Matthias Simon[14], Oliver Brüstle[2,7,15], Dennis A. Steindler[16], and Björn Scheffler[1,2,7,17]

Abstract

Purpose: Investigation of clonal heterogeneity may be key to understanding mechanisms of therapeutic failure in human cancer. However, little is known on the consequences of therapeutic intervention on the clonal composition of solid tumors.

Experimental Design: Here, we used 33 single cell–derived subclones generated from five clinical glioblastoma specimens for exploring intra- and interindividual spectra of drug resistance profiles *in vitro*. In a personalized setting, we explored whether differences in pharmacologic sensitivity among subclones could be employed to predict drug-dependent changes to the clonal composition of tumors.

Results: Subclones from individual tumors exhibited a remarkable heterogeneity of drug resistance to a library of potential antiglioblastoma compounds. A more comprehensive intratumoral analysis revealed that stable genetic and phenotypic characteristics of coexisting subclones could be correlated with distinct drug sensitivity profiles. The data obtained from differential drug response analysis could be employed to predict clonal population shifts within the naïve parental tumor *in vitro* and in orthotopic xenografts. Furthermore, the value of pharmacologic profiles could be shown for establishing rational strategies for individualized secondary lines of treatment.

Conclusions: Our data provide a previously unrecognized strategy for revealing functional consequences of intratumor heterogeneity by enabling predictive modeling of treatment-related subclone dynamics in human glioblastoma. *Clin Cancer Res; 23(2); 562–74. ©2016 AACR.*

Introduction

Cellular heterogeneity has traditionally been viewed as a result of hyperproliferation and increasing genetic instability that, at late stages of tumor progression, leads to the spawning of subclones (1, 2). Their phylogeny can be recapitulated, for example, by applying single-nucleus deep sequencing, regional dissections, or visualization of specific genetic hallmarks (3–5). On a practical note, increasing degrees of intratumor heterogeneity are acknowledged as an indicator for unfavorable disease progression/prognosis (6–8), and it is thought that heterogeneity data could have the potential to influence clinical decision making (9), but this is not routinely applied in the field yet. One aspect is a lack of preclinical model systems that could help to better understand the impact of chemotherapy on clonal heterogeneity. Ideal models

[1]Stem Cell Pathologies, University of Bonn Medical Center, Bonn, Germany. [2]Institute of Reconstructive Neurobiology, University of Bonn Medical Center, Bonn, Germany. [3]Department of Neurosurgery, University of Florida, Gainesville, Florida. [4]Department of Cellular & Molecular Medicine, Cleveland Clinic Lerner Research Institute, Cleveland, Ohio. [5]Institute for Medical Biometry, Informatics & Epidemiology, University of Bonn, Bonn, Germany. [6]Department of Neuroradiology, NYU Langone Medical Center, New York, New York. [7]LIFE & BRAIN GmbH, Bonn, Germany. [8]Cancer Therapeutics and Stratified Oncology, Genome Institute of Singapore, Singapore. [9]Division of Medical Genetics, University of Basel, Basel, Switzerland. [10]Health Cancer Center at Orlando Health, University of Florida, Orlando, Florida. [11]Department of Neuropathology, University of Bonn Medical Center, Bonn, Germany. [12]Department of Neurosurgery and Center for Stem Cell & Regenerative Medicine, The Brown Foundation Institute of Molecular Medicine, The University of Texas Health Science Center at Houston, Texas. [13]Department of Pathology, Immunology, & Lab Medicine, University of Florida, Gainesville, Florida. [14]Department of Neurosurgery, University of Bonn Medical Center, Bonn, Germany. [15]DZNE – German Center for Neurodegenerative Disease, Bonn, Germany. [16]JM USDA Human Nutrition Research Center on Aging, Tufts University, Boston, Massachusetts. [17]DKFZ-Division of Translational Oncology/Neurooncology, German Cancer Consortium (DKTK), Heidelberg & University Hospital Essen, Essen, Germany.

Note: Supplementary data for this article are available at Clinical Cancer Research Online (http://clincancerres.aacrjournals.org/).

D.A. Steindler and B. Scheffler are last authors of this article.

Corresponding Author: Björn Scheffler, University of Bonn, Sigmund Freud Strasse 25, Bonn 53127, Germany. Phone: 4922-8688-5473; Fax: 4922-8688-5443; E-mail: b.scheffler@dkfz.de.

doi: 10.1158/1078-0432.CCR-15-2089

Translational Relevance

Inevitably recurring tumor growth complicates even the most promising pharmacotherapies in glioblastoma. Arguing that coexisting cellular hierarchies contributing to pharmacoresistance are extractable from clinical samples, we here show that phenotypic and genetic stability of intratumor subclones enables controlled and discriminative drug profiling *ex vivo*. Our data imply that the respective profiles are directly applicable to predict intratumoral treatment-induced clonal population shifts *in vitro* and *in vivo*, and thus to predict the cellular composition of relapsing human cancer tissue at the time of primary diagnosis. In addition, we show that pharmacologic profiles could serve as a valuable asset for defining combinatorial secondary lines of treatment. Further development of this strategy may be key to the understanding of therapeutic failure, and it may become a sophisticated evidence-based planning tool for personalizing therapy in glioblastoma.

would have to implement genetic/phenotypic identity of subclones with the respective cellular function for monitoring drug effects over time in a given tumor (10).

In many of the particularly malignant cancers, for example, the primary brain tumor glioblastoma, (stem-like) subclones with intrinsic drug resistance are considered to account for treatment failure and relapse that inevitably occur during the course of disease (11–13). Recent insights from *in vitro* studies on intraindividual drug response suggest that subclones with differential resistance profiles coexist in glioblastoma (14). Here, we found that single cell–derived subclones of clinical glioblastoma samples maintain their distinct phenotypic and genetic identities *ex vivo* and that their pharmacologic profiles enable experimental access to model specific subclone targeting *in vitro* and *in vivo*. As a consequence, drug-related polyclonal population dynamics becomes predictable. A major further benefit of this approach is the previously unrecognized feature to identify subclone-specific drug combinations suited for sequential targeting of coexisting tumor cell hierarchies, which reflect the foundation of intratumor heterogeneity.

Materials and Methods

Tissue samples

Tumor tissue was obtained from glioblastoma surgery at the University of Bonn (BN035-BN118, Bonn, Germany) and the University of Florida (GNV019, Gainesville, FL, patient details: Supplementary Table S1). Local ethics committees at both sites approved the studies, and patients or their guardians provided informed consent. Tissue diagnosis/grading is based on the WHO classification (15, 16).

Tissue handling and cell culture

Handling of tissue and cell derivation protocols (BN035-BN118/GNV019) were described previously (17, 18). Samples were analyzed at *in vitro* passages 5 to 13. Subclones derived from passage 5/6 parental cells were investigated at subsequent *in vitro* passages 2 to 8. With the exception of neurosphere and extreme limiting dilution assays (ELDA), samples were grown adherently on laminin (Life Technologies)/poly-L-ornithine (Sigma-Aldrich)–coated (PO) plasticware (17, 18). Culture methods for reference/control cells were described: U87(MG) glioma cell line, hnNCs (human nonmalignant neural cells: short-term expanded hippocampus-derived adult human neural progenitors; ref. 18), and hESCdNPs (human ES cell–derived neural progenitor cells; ref. 19). Cell line authentication was conducted by the DSMZ using STR analysis, last tested in September 2015 [U87(MG)]. Human primary fibroblasts were provided by Dr. Phillip Koch and expanded in DMEM/F12 media (Life Technologies) supplemented with 10% FCS (Hyclone, GE Healthcare) and 1% antibiotic-antimycotic. All investigated cells tested mycoplasma negative per standard cell lysate PCR detection. For *in vitro* growth kinetics, populations doublings (PD) were calculated: $n = 3.32$ (log UCY – log I) + X, where n = final PD number at the end of given subculture; UCY = cell yield at that point; I = cell number used as inoculum of subculture; X = doubling level of inoculum used to initiate the quantified subculture. The neurosphere assay testing cellular differentiation was applied as described previously (17, 20). For the ELDA, GNV019 cells plated in a volume of 150 μL on ultralow attachment 96-well plates (Corning) in decreasing numbers for 7 days were incubated with Calcein AM viability dye (5 μmol/L) for 30 minutes to label vital cells and for fluorescence-based quantification of tumor spheres.

Derivation of tumor subclones

Passage 5 GNV019 cells were plated at 15 cells/cm^2 on five PO-coated 10-cm dishes. Twenty individual cells per dish were randomly selected on the subsequent day, marked with pen at the bottom of the dish, and followed for 30 to 60 days. Seven of these formed clonal colonies, were selected using 8-mm cloning cylinders (Corning), trypsinized, and transferred to a 6-cm dish for expansion. CL1/2/3/6/7 cells were depicted from these based on their distinctive morphologies. BN samples were plated at 0.5 cells per well in up to eight 96-well plates, validated, and monitored throughout clonal expansion by automated image-based analysis (Cellavista, Roche). Eleven to 26 single cell–derived subclones were selected per case and expanded. For generation of pilot data, at least 5 subclones were used per patient sample.

Compound screening and treatment

Reference/control cells, parental tumor cells, and subclones were seeded in 96-well plates at 5–13 × 10^3 cells/cm^2 in triplicates. Twenty-four hours later, drugs were applied as 10× stock dilutions. Cellular viability was determined as the ratio of background-subtracted alamarBlue (Life Technologies) fluorescence intensities of treated and vehicle control cells. Compounds of the pilot drug screen (Supplementary Table S2) were applied in six different concentrations to determine dose–response levels. Four days later, cellular viability was compared with vehicle applications [0.55% DMSO for compounds combined with 50 μmol/L temozolomide; 1.5% DMSO for temozolomide treatment alone; 0.5% ethanol (EtOH) for perifosine, and 0.5% DMSO for all other drugs]. The "Killer Plates" compound library (MicroSource) was applied to GNV019 cells at 1 μmol/L concentrations each and compared with vehicle controls (0.01% DMSO) at 5 days after treatment. IC_{50} evaluation for selected compounds was performed as described previously (18).

For coculture, subclones were labeled with green (CellTracker Green CMFDA, 5 μmol/L, or Vybrant DiO, 1:200) or red fluorescent dyes (CellTracker Red CMTPX, 25 μmol/L, or Vybrant DiD,

1:200, all Life Technologies) for 30 minutes. Equal quantities of green- and red-labeled cells were seeded on 12-well plates. CL1/2/3/6/7 cells were treated with 10 μmol/L thioguanine, 2 μmol/L oridonin, 4 μmol/L sorafenib, 1 μmol/L cantharidin, or 0.1% DMSO for 5 days. BN035 subclones were treated with 0.4 nmol/L bortezomib, 8 μmol/L lonafarnib (+50 μmol/L temozolomide), or 0.25% DMSO. BN046 subclones were treated with 3 μmol/L 17-AAG, 10 μmol/L etoposide (+50 μmol/L temozolomide), or 0.15% DMSO for 3 days. Challenged cells were trypsinized for flow cytometry using 15–20 $\times$ 10^3 cells (FACSCalibur Cell Analyzer; BD Biosciences) to determine drug effects.

For subclone selection from parental GNV019 cells, increasing concentrations of thioguanine or 0.1% DMSO were applied for 5 days, followed by a 4-day growth factor withdrawal-induced differentiation period, before quantifying (giant) multinucleated cells. CL2-like cells were selected by single- or repeated treatment with 4 μmol/L sorafenib for 5 days. For subclone selection from BN035 and BN046 parental cells, drugs were applied in two 3-day cycles at concentrations indicated (Supplementary Figs. S5B and S6B). Sequential treatment (5 + 5 days for all) of GNV019 cells (Fig. 6) was either conducted with 10 μmol/L thioguanine/0.1% DMSO (first line), followed by 20 μmol/L perifosine, 1.5 μmol/L SAHA (+50 μmol/L temozolomide), 3 μmol/L sunitinib, 0.5 nmol/L bortezomib, 100 nmol/L dasatinib, or 0.12% DMSO (second line). The alternative course included 4 μmol/L sorafenib/0.02% DMSO (first line), followed by 1 μmol/L cantharidin, 20 μmol/L imatinib, 0.5 μmol/L etoposide (+50 μmol/L temozolomide), 0.2% DMSO, 1 mmol/L temozolomide, or 1% DMSO (control condition for temozolomide alone; second line).

Orthotopic xenograft experiments and animal treatments

Ethical Committees of the Universities of Bonn and Florida approved all animal studies. For engraftment, cells were harvested, counted, and resuspended in 0.1% DNase I (Worthington)/PBS (Life Technologies). Cell vitality was confirmed via Trypan blue exclusion. Two microliters encompassing 1 $\times$ 10^5 cells were stereotactically applied to the brains of Fox Chase SCID/beige mice (females, 9–13 weeks old; 1.6 mm anterior, 1.9 mm lateral to the bregma, 1.4 mm deep from the dura; Charles River Laboratories). In addition to presented data, tumorigenicity and cellular characteristics of GNV019 parental and subclonal cells were confirmed in NMRI nu/nu mice (females, 6–10 weeks old; $n = 2$, each; 2.2 mm anterior, 1.3 mm lateral, 1.7 mm deep; Janvier Labs). Mice were monitored daily and euthanized when signs of neurologic impairment or significant weight loss ($\geq$20% from preoperative weight) were noted. For routine histology, brains were fixed by vascular perfusion (4% formaldehyde). Coronal gradient echo, T2-weighted, and fluid-attenuated inversion recovery MRI data were obtained from formaldehyde-fixed whole brains using the core facility of the McKnight Brain Institute (University of Florida, Gainesville, FL) under standard imaging protocols with a 15-mm birdcage coil and 11-T horizontal-bore magnet (Bruker).

In vivo analysis of subclone enrichment commenced at day 42 postorthotopic xenotransplantation of GNV019 parental cells. A 2.5 mg/mL stock solution of thioguanine (50 mg thioguanine/20 mL of 0.02 mol/L NaOH) generated doses of 10 mg/kg per injection and was applied for 3 consecutive days (21). A total of 100 mg sorafenib dissolved in 2.5 mL Kolliphor/EtOH (50:50, Sigma-Aldrich) to obtain a 4$\times$ stock solution was further diluted in ddH_2O. Treatments (100 mg/kg) were conducted on 5 days per week (22). Sorafenib-induced population shifts were assessed using DNA from 5 of 8 animals of the experimental series (2$\times$ Kolliphor/EtOH, 3$\times$ sorafenib). Three of 8 samples were excluded because sufficient DNA quantity/quality could not be obtained: two samples representing prenecrotic brain tissue of animals that died over night; one sample failed DNA extraction.

Immunocytochemistry

Paraformaldehyde-fixed cells and formaldehyde-fixed paraffin-embedded tissues were supplied with primary antibodies against βIII-tubulin (Promega; monoclonal mouse, clone 5G8, 1:1,000), GFAP (DAKO; polyclonal rabbit, #Z0334, 1:600), pan-cadherin (Thermo Fisher Scientific, polyclonal rabbit; #PA5-19479, 1:200), and α-tubulin (Sigma-Aldrich, monoclonal mouse; clone DM1A; 1:1,000) overnight at 4°C. Respective antigens were labeled by incubation with fluorophore-conjugated secondary antibodies (Alexa Fluor 488 goat anti-mouse IgG 1:800 and Alexa Fluor 555 goat anti-rabbit IgG 1:500, Life Technologies) for 1 hour at room temperature. Cell nuclei were exposed with 2 μg/mL DAPI (Sigma Aldrich) for 10 minutes. Fluorescence microscopy was performed on a Zeiss Axioskop2 or Axio Imager.Z1 upright microscope. Frequencies of multinucleated giant cells (mGC; *in vivo*) and mGC-like multinucleated cells (mnCells; *in vitro*) were determined by quantifying mono- versus multinucleated cells in respective samples using DAPI and α-tubulin (*in vitro*) or pan-cadherin (*in vivo*) labeling. Quantification was conducted by averaging the results of at least two investigators (R. Reinartz, L. Rauschenbach, and B. Scheffler) blinded to the experimental conditions.

Molecular biology

DNA/RNA was isolated using the AllPrep DNA/RNA Mini Kit (Qiagen) following the manufacturer's instructions. Chromosomal aberrations were analyzed using Illumina's BeadChips (HumanHap550/Human610-Quad). Sample preparation was performed according to Illumina's Infinium protocols. For whole-genome gene expression profiling, total RNA of biological triplicates was extracted using QIAzol Lysis Reagent (Qiagen) and analyzed using HumanHT-12 v3 expression BeadChips (Illumina). Gene expression and genotyping data were deposited at GEO (Gene Expression Omnibus: accession numbers GSE72927, GSE72732). *TP53* mutation screening was performed according to the direct sequencing protocol of the International Agency for Research on Cancer (Lyon, France). DNA copy numbers were quantified on a ViiA 7 Real-Time PCR System (Life Technologies) using SYBR Green. PCR cycling conditions are as follows: 95°C for 3 minutes, followed by 40 cycles at 95°C for 20 seconds, 60°C for 20 seconds, and 72°C for 30 seconds. C_t values for target genes on Chr. 1 (*CDKN2C*), Chr. 5 (*SCAMP1*, *CHD1*), and Chr. 22 (*BID*, *NF2*) were normalized using C_t values of the Chr. 2 reference genes (*MEMO1* and *ASB3*). Copy number values were calculated using the $\Delta\Delta C_t$ method on tumor samples and human leukocyte DNA as reference. Gene expression analysis of signature neural stem-like genes was performed as described previously (18) using 1 μg total RNA (for primers, see Supplementary Table S3). Custom multiplex ligation-dependent probe amplification (MLPA) kits (P345-X1 & P346-X1; MRC-Holland) were used to detect copy number alterations in BN035 and BN046 cells. A total of 90 ng DNA from tumor cells or from (two individual) reference human leukocyte DNA was used for each MLPA reaction. Fragment separation was performed on a 3130xl Genetic Analyzer (Applied

Biosystems) and MLPA ratios determined using Coffalyser software (MRC-Holland).

Bioinformatics and statistical analysis

Hierarchical clustering, calculation of Pearson correlation coefficients, heatmaps, and logR ratio plots were performed using R-project statistical software (v3.0.2; ref. 23). Molecular subtypes of GNV019 samples were classified as "neural" (according to ref. 24). Cluster dendrograms were created using Euclidean distance and average linkage analysis. All other computations were carried out using GraphPad Prism 6.0f and Microsoft Excel. Where applicable, the two-tailed Student *t* test (assuming equal variances), the one-way ANOVA with Tukey correction for multiple comparisons, or the two-way ANOVA with Bonferroni correction for multiple comparisons were performed for statistical analysis. Standard distribution of data was applied for respective tests. Data analysis is based on biological triplicates, unless otherwise specified. Unless otherwise indicated, data are presented as mean ± SD (levels of significance: *, $P < 0.05$; **, $P < 0.01$; ***, $P < 0.001$; ****, $P < 0.0001$). Cartoons were produced using SERVIER Medical Art.

Results

Drug–response profiles of tumor subclones reflect intra- and interindividual tumor heterogeneity

In pilot experiments, we explored single cell–derived (subclonal) cultures from clinical patient samples to display heterogeneity of drug–response patterns. On the basis of reported transcriptome analysis of 430 single cells from 5 glioblastoma patients (25), we expected patterns of strong interindividual differences and a considerable degree of intratumor heterogeneity. In a parallel constellation, we applied short-term expanded primary cell cultures from five glioblastoma patients and, additionally, a total of 33 respective subclones for analysis of differential drug response. All cells were maintained under adherent *in vitro* conditions suited for the expansion of neural stem- and precursor cells (Materials and Methods). Twenty clinical trial grade drugs and compounds (Supplementary Table S2) were used to determine IC_{50} values, that is, the individual concentrations that reduced cellular viability by 50% compared with vehicle control treatments. Hierarchical clustering of data revealed an extent and pattern of heterogeneity comparable with the transcriptome data presented by Patel and colleagues (25). A strong interindividual variability was noted as well as substantial intraindividual differences of drug–response patterns (Fig. 1). Notably, for each of the five cases, the median drug concentration difference between the most and least resistant subclone revealed a 2-fold intraindividual variability of drug response among all investigated compounds (Supplementary Fig. S1, mean factor, 2.32; range, 1.86–2.92).

Thus, data from our test system indicated considerable variation of drug responsiveness among intratumor subclones, adding another level of complexity to the interindividual differences that are commonly acknowledged in the biology of glioblastoma

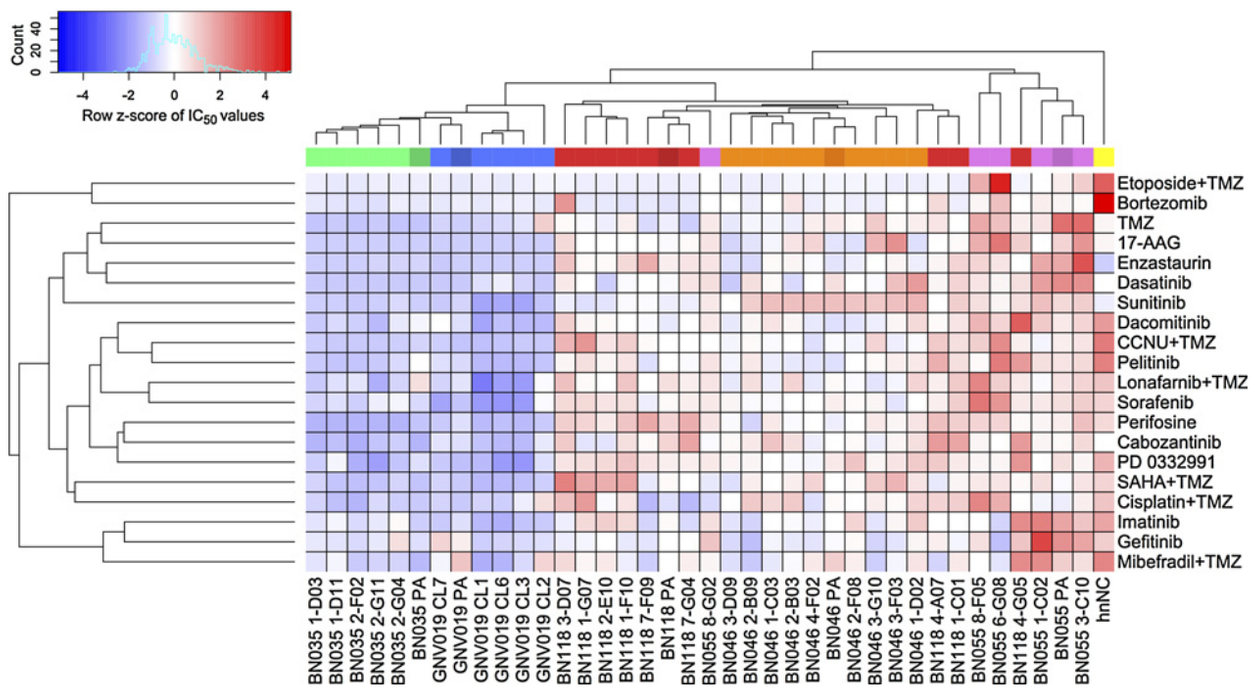

Figure 1.

Pilot data: drug–response profiles of tumor subclones reflect intra- and interindividual tumor heterogeneity. Unsupervised clustering of z-score–transformed IC_{50} data. Column color code identifies five glioblastoma cases, their respective parental cultures (i.e., one dark shade per color), and their respective subclones (light shades). Data matrix codes reflect low (blue) versus high (red) IC_{50} values. Consistency of results was verified by correlating triplicate analysis of two individual library batches ($R^2 = 0.994$). hnNCs, human nonmalignant brain cells (see Materials and Methods). For individual results and drug/compound details, see Supplementary Fig. S1 and Supplementary Table S2. Note considerable variability of intertumor (29/33 subclones grouped within their patient-specific cluster) and intratumor (4/33 subclones even presented as outliers clustering "transindividually") drug responses. TMZ, temozolomide.

(24, 26). These pilot data, however, also raised questions: on one hand related to the overall range of potentially coexisting subclones and intraindividual drug–response profiles; on the other hand, it was unclear to what degree the subclones maintain their distinct phenotypic and genetic identities *ex vivo* and whether the determined variability of drug response would impact on the cellular composition of a tumor bulk upon treatment. We prioritized investigation of the latter complex of questions, because the range of intratumor response profiles would be irrelevant if significant alterations to the cellular composition of the tumor bulk would not occur.

Morphologic, genetic, and functional traits of tumor subclones are preserved *in vitro* and *in vivo*

Previous studies already demonstrated that patient- and disease-specific hallmarks of glioblastoma could be mirrored *ex vivo* for experimental investigation (17, 18, 27). For experimental access to studying consequences of clonal diversity, we selected the case GNV019 that presented with a characteristic morphologic trait of heterogeneity: mGCs. Their presence is not an obligatory finding, but rare mGCs are frequently observed in glioblastoma (16). Histopathology of the patient's tumor accordingly revealed very few (≈1%) mGCs intermixed with other pleomorphic smaller cell phenotypes (Fig. 2A). Morphologic heterogeneity was similarly observed when primary GNV019 cells were isolated and propagated under adherent conditions (Fig. 2B; ref. 20). The cellular expansion rate remained stable, and the disease- and patient-specific gene expression-/copy number profiles were conserved *in vitro* (Fig. 2C–E; refs. 28, 29). Orthotopic xenotransplantation demonstrated a tumorigenic potential replicating the original tumor's glioblastoma histology, including the presence of intermixed, rare mGCs (2.1 ± 1.1%; $n = 11$; Fig. 2F, G, and I). We next investigated subclones (CL1/2/3/6/7) derived from early-passage parental GNV019 cells (Fig. 2H, top). They presented common genomic profiles with only a few differential copy number alterations (Supplementary Fig. S2), and similar to the parental samples, they each classified as "neural" subtype (24). Notably, however, orthotopic xenotransplantation revealed distinct categories of *in vivo* behavior. CL2 cells were not tumorigenic ($n = 11/11$). The other subclones consistently developed histopathologic features of glioblastoma (16), yet their cellular composition varied. CL7-derived tumors appeared "small cell-enriched": most tumor cells were uniformly small and round, mGCs extremely rare (0.2 ± 0.2%; $n = 8$). In contrast, CL1/3/6-derived tumors presented high mGC frequencies (32.8 ± 9.3%; $n = 8/7/10$; Fig. 2H, bottom, and I).

We concluded that GNV019 disease- and patient-specific characteristics were preserved *ex vivo* and that isolation of tumor subclones enabled functional access to distinguishable morphologic characteristics of the parental tumor.

Subclone phenotypes present distinct developmental and genetic traits

We next explored whether the distinct categories of *in vivo* behavior reflected distinct patterns of cellular plasticity, gene expression, and genetic aberrations. *In vitro,* the subclones consistently revealed stem-like developmental potentials, that is, 5 of 5 were able to self-renew (Supplementary Fig. S3) and to differentiate into neuronal and glial progeny (Fig. 3A, top). Notably, a pronounced capacity to also generate (giant) mnCells upon spontaneous differentiation *in vitro* that resembled mGCs *in vivo* was only observed in CL1/3/6 cells matching their developmental potential in xenografts (Fig. 3A, bottom). Moreover, analysis of signature neural stem-like genes (*FABP7*, *OTX2*, *SOX9*, *BMI1*, *SOX2*, *VIM*, *NOTCH2*, *VCAM1*, *NES*, *NCAM1*, *SOX8*, and *FGFR4*) indicated distinct expression motives separating nontumorigenic CL2 cells from tumorigenic mGC-forming CL1/3/6, and from tumorigenic "small cell-enriching" CL7 cells (Supplementary Fig. S4). Unsupervised clustering of correlation data from genome-wide gene expression and in-depth genotype analysis further confirmed the specific hierarchic alignment of GNV019 subclones (Fig. 3B).

In synthesis, findings indicated consistently distinct morphologic, developmental, and genetic traits of the investigated GNV019 subclones *in vitro* and *in vivo*, serving as an ideal basis to reveal functional consequences of intratumor heterogeneity.

Distinct pharmacologic response patterns enable selection of subclones by *in vitro* drug challenge

The specific alignment of CL1/3/6, CL2, and CL7, as determined in the functional and molecular classification experiments above, corresponded directly to the drug response profiles of GNV019-derived subclones of our pilot data (Fig. 1). This encouraged further investigation toward pharmacologic targeting of distinct subclones. To broaden the approach and for experimental validation, we additionally applied a commercial library comprising 160 synthetic/natural compounds, previously used for identification of new drug candidates in glioblastoma (18). Hierarchical clustering of the respective cellular viability data further confirmed the specific alignment of CL1/3/6, CL2, and CL7 (Fig. 4A).

Together, data suggested that the five investigated GNV019 subclones represented three independent intratumor cell hierarchies separating coexisting precursor cells and their descendants by functional, phenotypic, and genetic traits. We hypothesized that these hierarchies needed to be considered as functionally distinct intratumor cell populations with independent drug resistance profiles. On the basis of this assumption and the noted stability of subclones *ex vivo*, we opted for discriminative investigation and modeling of intratumor population dynamics using GNV019 cells as an experimental system. The approach was initiated by determining the most suitable drugs for pharmacologic hierarchy selection, chosen from both sets of compound screening data (Fig. 4B). Subsequent pharmacodynamic analysis established drug concentrations with most pronounced effects. The highest differential level of intrinsic drug resistance was defined at 10 μmol/L thioguanine (synthetic guanosine analogue antimetabolite, inhibits nucleic acid synthesis) for CL1/3/6 and at 2 μmol/L oridonin (mechanism of action not yet fully understood) for CL7 cells. CL2 cells could be discriminated from all others by their sensitivity to 1 μmol/L cantharidin (PP2A inhibitor) and by their resistance to 4 μmol/L sorafenib (multikinase inhibitor, see Supplementary Table S2; Fig. 4C). To test the drugs' applicability for pharmacologic selection, defined mixtures of fluorescently prelabeled subclones were exposed in coculture to a single drug dose, and their respective population shifts were evaluated by flow cytometry 5 days later (Fig. 4D and E). Comparison with vehicle controls confirmed the predicted targeting of distinct subclones/hierarchies. The resulting mean population

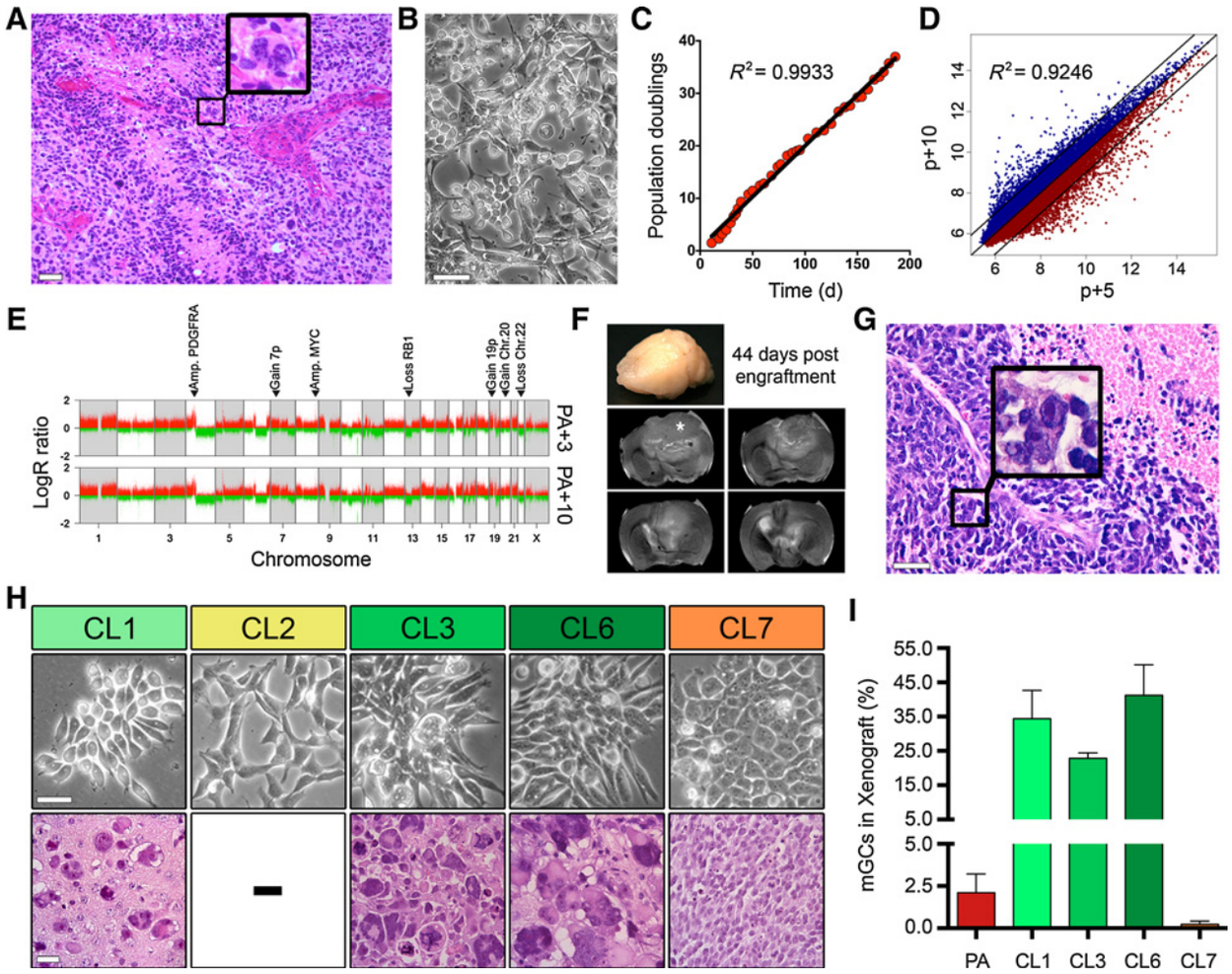

Figure 2.

Morphologic, genetic, and functional traits of tumor subclones are preserved *in vitro* and *in vivo*. **A,** H&E–stained original tissue biopsy (case GNV019) diagnosed as glioblastoma. Typical necrosis, microvascular proliferation, and mitotically active glial cells are present. Note the rare mGCs (example highlighted in box). **B** and **C,** Phase contrast appearance of GNV019 parental cells (**B**) and respective growth kinetics for 35 passages *in vitro* (**C**). **D,** Scatterplot of log2-transformed whole-genome gene expression data from passage 5 and passage 10 GNV019 parental cells revealing high correlation. A total of 96.8% of all expressed genes are found within the 2-fold demarcated area. **E,** LogR ratio plots illustrating glioblastoma-type aberrations (28, 29) from passage 3 versus passage 10 GNV019 parental cells. Note the overlap. **F,** Serial coronal T2-weighted MRI of an *ex vivo* recipient SCID-beige mouse whole brain demonstrating development of a large T2-intermediate mass infiltrating left frontal cortex and subjacent basal ganglia 44 days after xenografting GNV019 parental cells [asterisk (*), original transplant site]. There is herniation and midline shift from substantial mass effect. **G,** Microscopic appearance of the respective xenograft (H&E, tissue section). Note the similarity of pathology to the original patient specimen (**A**). One of the rare mGCs is exposed (box). **H,** Subclones derived from GNV019 parental cells at passage 5. Top, their phase contrast appearance *in vitro*; bottom, H&E stains expose distinct xenograft morphologies. CL2 cells were not tumorigenic. **I,** distribution of mGCs in respective xenografts. For quantification, a mean of 10,145 cells were counted in 3 to 10 random 40× fields per case. PA, GNV019 parental cells. Scale bars, 250 μm (**A**), 50 μm (**B** and **H**), and 100 μm (**G**). Also see Supplementary Fig. S2. TMZ, temozolomide.

shifts were determined at 20 ± 3% in response to *in vitro* drug challenge (Fig. 4F).

Intratumoral, treatment-related population dynamics can be predicted *in vitro*

The aforementioned, reductionist coculture experiments suggested that the ratios of intratumoral subclone fractions could be selectively modulated depending on the choice of drug used for pharmacologic challenge. In the next series of experiments, we aimed to show that this could be applied to the more complex setting of parental GNV019 cells.

In the first approach, parental cells were considered as a polyclonal collection of precursors either responsible for (e.g., thioguanine-resistant CL1/3/6-like cells) or incapable of mGC/mnCell generation (e.g., thioguanine-sensitive CL2/7-like cells; Fig. 5A). The morphologic trait of mGC/mnCell generation was used as a read-out parameter to quantify the extent of pharmacologic selection. Application of thioguanine to GNV019 parental cells and subsequent differentiation *in vitro* indeed yielded up to 5-fold concentration-dependent increases of mnCell fractions (Fig. 5B). The corresponding increases correlated with differential viability effects recorded at pharmacodynamic

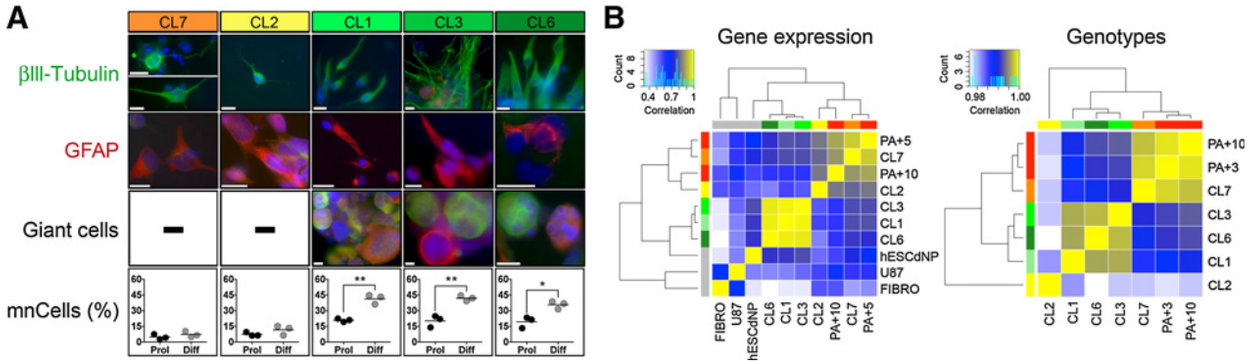

Figure 3.

Subclone phenotypes present distinct developmental and genetic traits. **A,** Neurosphere assay (Materials and Methods) testing the differentiation potential of GNV019 subclones *in vitro*. Secondary neurospheres derived from individual subclones were plated and analyzed 10 to 26 days after growth factor withdrawal. Spontaneous differentiation always yielded neuronal (βIII-tubulin$^+$) and glial (GFAP$^+$) progeny. Quantification of (giant) mnCells based on counting 1,158 ± 172 cells per condition, that is, proliferative (Prol) versus 4-day growth factor withdrawal (Diff) *in vitro* ($n = 3$ independent experiments, each). **B,** Correlation heatmaps of gene expression and genotype data. Left, to focus on transcriptional differences, the 1,000 most variably expressed genes were identified from genome-wide gene expression datasets of GNV019 parental cells and subclones/hESCdNPs/U87 and human fibroblasts (Materials and Methods). Expression values of these genes were correlated between all samples, and respective Pearson correlation coefficients from every single correlation analysis were illustrated as heatmap and clustered using Euclidean distance and average linkage analysis; right, B allele frequency values (550,316) from the SNP array dataset (Materials and Methods) were correlated between all case GNV019 samples. Pearson correlation values from every single correlation analysis were then illustrated as heatmap and clustered using Euclidean distance and average linkage analysis. Note the high correlation values. Color keys, Pearson correlation values. Note the consistent alignment of tumor subclones. PA+3/5/10, GNV019 parental cells at the respective cell culture passage. FIBRO, human fibroblasts; U87, glioma cell line; hESCdNP, noncancerous human ES cell–derived neural precursor cells (19). Scale bar, 20 μm (**A**). Significance levels: *, $P < 0.05$; **, $P < 0.01$. Also see Supplementary Fig. S4.

investigation of CL1/3/6 and parental cells (Fig. 5C and D, compare Fig. 4C). In a control setting, we confirmed that thioguanine alone did not induce the mnCell phenotype, as its application did not alter the capability of CL2 or CL7 cells to develop the phenotype *in vitro* (Fig. 5E). We concluded that, as predicted, thioguanine selectively enriched CL1/3/6-like cells from the GNV019 parental cells. The second approach was based on the presence of a distinctive, 36-megabase deletion in CL2 cells on chromosome 5q (Fig. 5F). Used as a read-out parameter, a decreased abundance of this chromosomal region would indicate an increased fraction of CL2-like cells within the GNV019 parental cells (Fig. 5G). The extent of pharmacologic selection was then determined by quantifying copy numbers of genes within the CL2-specific deletion. As predicted, sorafenib exposure led to dose-dependent copy number decreases, indicating an enrichment of CL2-like cells from GNV019 parental cells (Fig. 5H, compare Fig. 4C).

These data implied that pharmacologic profiling of subclones could blueprint *post hoc* identification of individual cell hierarchies in a heterogeneous parental tumor sample. To validate whether this insight could be applied to other glioblastoma specimens, we investigated 14 additional subclones from two more clinical samples of our pilot dataset (Fig. 1), adopting the experimental course established on GNV019 cells. Briefly, BN035- and BN046 subclones underwent MLPA analysis for identification of specific genetic marks (Materials and Methods), selection of subclone-specific drugs from pharmacologic profiles, respective validation in coculture, and successful tracking of predicted subclone enrichment in parental tumor samples (Supplementary Figs. S5 and S6). The consistency of experimental results from all three investigated clinical samples led us conclude that intratumoral, treatment-related cellular population dynamics is predictable, based on discriminative investigation of drug responses under controlled *in vitro* conditions.

Intratumoral, treatment-related population dynamics can be predicted *in vivo*

Next, orthotopic xenotransplantation validated predictability of drug-induced polyclonal dynamics *in vivo*. Treatments of animals engrafted with 10^5 GNV019 parental cells commenced at day 42, when intracerebral glioblastoma characteristics had already developed (compare Fig. 2F and G). Intraperitoneal vehicle injections yielded a median overall survival (mOS) of 60.5 days ($n = 3$, each; Fig. 5I).

The established morphologic/genetic read-out parameters were then used to verify thioguanine/sorafenib–induced enrichment of distinct hierarchies, that is, CL1/3/6-like or CL2-like cells. Both drugs indeed induced the predicted population shifts, independent of their influence on mOS. Thioguanine applications were limited to three injections due to potential myelotoxicity ($n = 6$ animals; intraperitoneal; 21) and did not extend the mOS of engrafted animals (Fig. 5I). Nevertheless, a significant 2.8-fold increase of mGCs indicated a treatment-related population shift as predicted ($P = 0.0149$; Fig. 5J). In the parallel experiment, sorafenib applications ($n = 5$ animals; intraperitoneal, dose according to ref. 22) extended the mOS significantly to 74 days ($P = 0.0042$; Fig. 5I). Microdissected tumor tissue from these animals then provided evidence for an increasing population size of CL2-like cells, as predicted. Quantifying copy numbers of genes in the CL2-specific region of deletion on chromosome 5q revealed a significant decrease from 2.03 ± 0.05 (vehicle) to 1.83 ± 0.06 (sorafenib; $P = 0.029$; Fig. 5K).

Implications of predictable population dynamics for second-line treatment strategies

In the last series of experiments, we investigated whether information from *ex vivo* pharmacologic profiling and prediction of subclone enrichment could be applied to the design of rational drug combinations. We hypothesized that one drug could be used

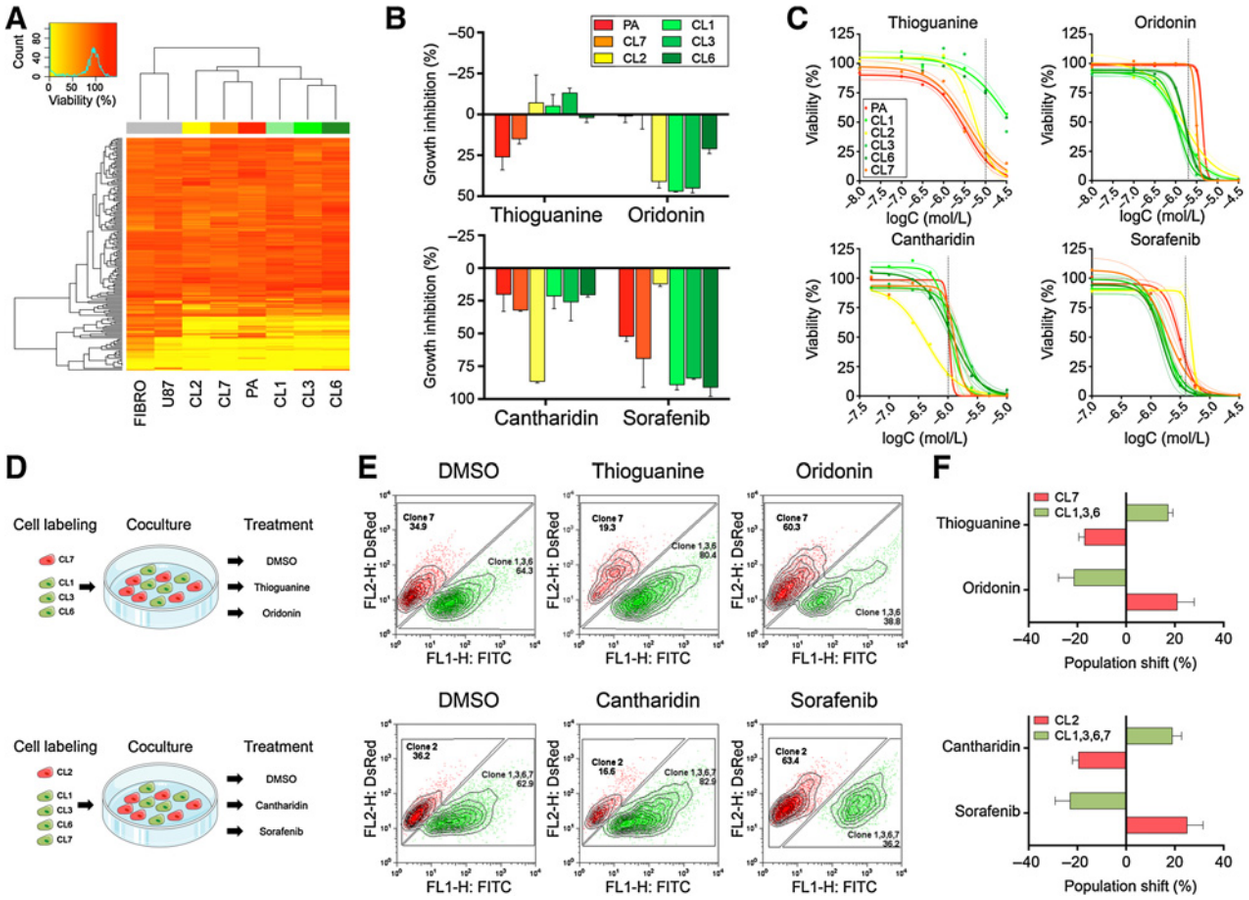

Figure 4.

Distinct pharmacologic response patterns enable selection of subclones by *in vitro* drug challenge. **A,** The "Killer Plates" collection was applied (1 μmol/L, each) to record pharmacologic responses of GNV019 cell samples. Heatmap, unsupervised clustered viability values (FIBRO, human fibroblasts; U87, glioma cell line; PA, GNV019 parental cells). **B,** Subset of data from **A**, including sorafenib (applied at 3.16 μmol/L) from set of pilot screening data, suggesting candidate compounds for pharmacologic selection of GNV019 subclones. Growth inhibition determined from viability analysis. **C,** Dose–response curves of candidate compounds. Colored dashed lines, 95% confidence interval of the nonlinear regression curve; dashed vertical lines, drug concentrations chosen for further pharmacologic selection studies. **D,** Experimental coculture paradigm. For each experiment, equal amounts of red versus green prelabeled GNV019 subclones were mixed and exposed to the indicated compounds. **E,** At 5 days after exposure, at least 15,000 cocultured cells were quantified by FACS analysis. Shown are representative plots indicating drug-induced shifts of population size among prelabeled subclones in coculture. **F,** Graphs depict the respective population shifts as calculated by subtracting the percentage of the DMSO-treated control cells from the drug-treated cells ($n = 3$ experiments, each).

in a first-line setting to drive the heterogeneous parental tumor bulk toward enrichment of particular subclones/hierarchies with distinct sensitivities to a choice of second-line drugs. The hypothesis was tested in two settings on GNV019 parental cells, implementing pharmacologic profiles as planning tools (Fig. 6A and C). In setting one, we observed enrichment of CL1/3/6-like cells with thioguanine, rendering the parental tumor bulk significantly more vulnerable to perifosine, SAHA + temozolomide, or sunitinib, which were predicted particularly effective on CL1/3/6 cells by the initial profiling. In contrast, drugs with minor inhibitory effects on CL1/3/6 cells in the initial profiling, for example, bortezomib and dasatinib, showed a less pronounced effect on bulk tumor cells secondary to thioguanine application (Fig. 6A and B). In setting two, enrichment of CL2-like cells with sorafenib required cantharidin for more effective second-line inhibition. As predicted from CL2 profiling, imatinib, etoposide + temozolomide, and temozolomide were less appropriate second-line combinations for sorafenib (Fig. 6C and D). In a control arm for both sets of experiments, we could furthermore show that these effects were exclusive to the parental bulk of tumor cells (Supplementary Fig. S7).

We conclude that *ex vivo* drug profiling of tumor subclones can facilitate predictions on treatment-related population dynamics and that rational drug combinations for sequential application in glioblastoma can be identified.

Discussion

Our study considers glioblastoma as a polyclonal collection of potent cellular hierarchies, at least at clinical manifestation of disease. The concept combines classic stochastic and cancer stem cell models (2, 12), implying that subclones with distinct intrinsic resistance profiles coexist in tumor specimens. Although poor or short-lasting therapy responses still occur in most glioblastoma

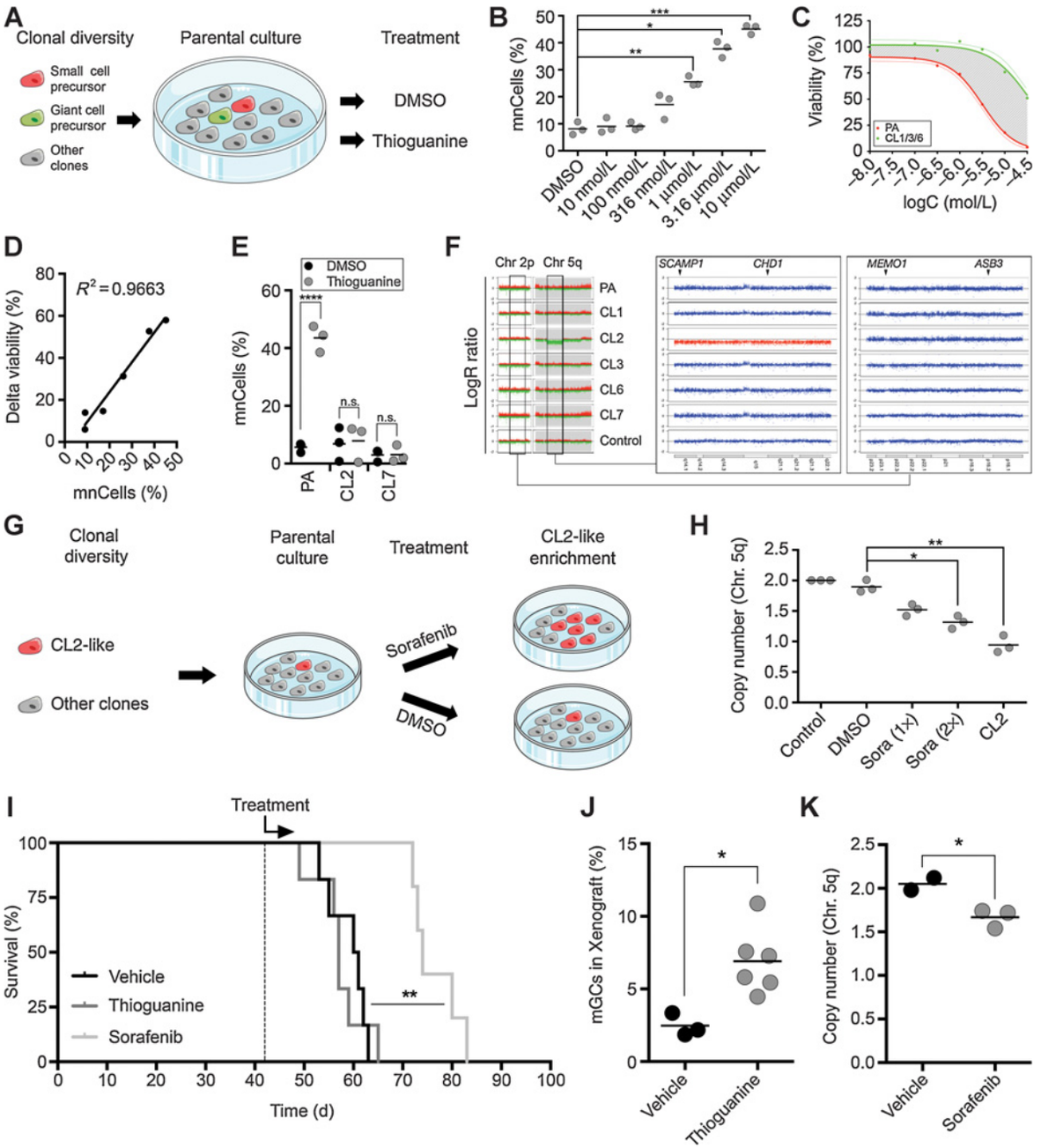

Figure 5.

Intratumoral, treatment-related population dynamics can be predicted *in vitro* (**A–H**) and *in vivo* (**I–K**). **A,** Paradigm using GNV019 parental cells for subclone enrichment experiments. **B,** Graph depicts rise of (giant) mnCell frequencies in response to increasing concentrations of thioguanine (5-day treatment plus 4-day differentiation). Quantification based on counting 306 ± 117 cells per condition ($n = 3$ experiments, each). **C,** Dose–response curve on GNV019 parental cells versus mean values from CL1/3/6 cells. Shaded area, difference between both curves (delta viability). **D,** Linear regression analysis correlating mnCell frequencies (from **B**) with delta viability (from **C**). **E,** Graph showing drug effects on CL2/7 cells versus GNV019 parental cells. Quantification of mnCells based on counting 674 ± 428 cells per condition ($n = 3$ experiments, each). **F,** LogR ratio plot (scale −2/+2) of CL2-specific deletion (middle, red: 5q14.1-q22.1). For qRT-PCR DNA copy number analysis, primers were designed for intra- (*SCAMP1*/*CHD1*) and extra (Chr. 2p23.2-16.1)-deletion genes (*MEMO1*/*ASB3*) as indicated. **G,** Paradigm using GNV019 parental cells for subclone enrichment experiments: Sorafenib (4 µmol/L) or DMSO (0.02%) was applied for 5 days (1–2 cycles), followed by DNA isolation for copy number quantification. **H,** Graph depicts respective copy number quantification data, normalized using normal human leukocyte DNA ($n = 3$ experiments, each). Sora, sorafenib. **I,** Kaplan–Meier graph illustrating initiation of treatment (dashed line) and survival times of animals xenotransplanted with GNV019 parental cells. The graph combines survival statistics for NaOH and Kolliphor/EtOH vehicle controls. Shown level of significance reflects Mantel–Cox test results for sorafenib- versus Kolliphor/EtOH–treated animals. **J,** Graph depicts blinded quantification of mGCs in vehicle (0.02 mol/L NaOH, $n = 3$) versus thioguanine (3 × 10 mg/kg, $n = 6$)–treated animals sacrificed at the end of the experiment. **K,** Graph depicts qRT-PCR DNA copy number analysis conducted in analogy to **H**. Microdissected tissue derived from animals treated with sorafenib (100 mg/kg, $n = 3$) was compared with tissue from Kolliphor/EtOH–treated (12.5%/12.5% in ddH2O, $n = 2$) animals. Significance levels: *, $P < 0.05$; **, $P < 0.01$; ***, $P < 0.001$; ****, $P < 0.0001$. n.s., not significant.

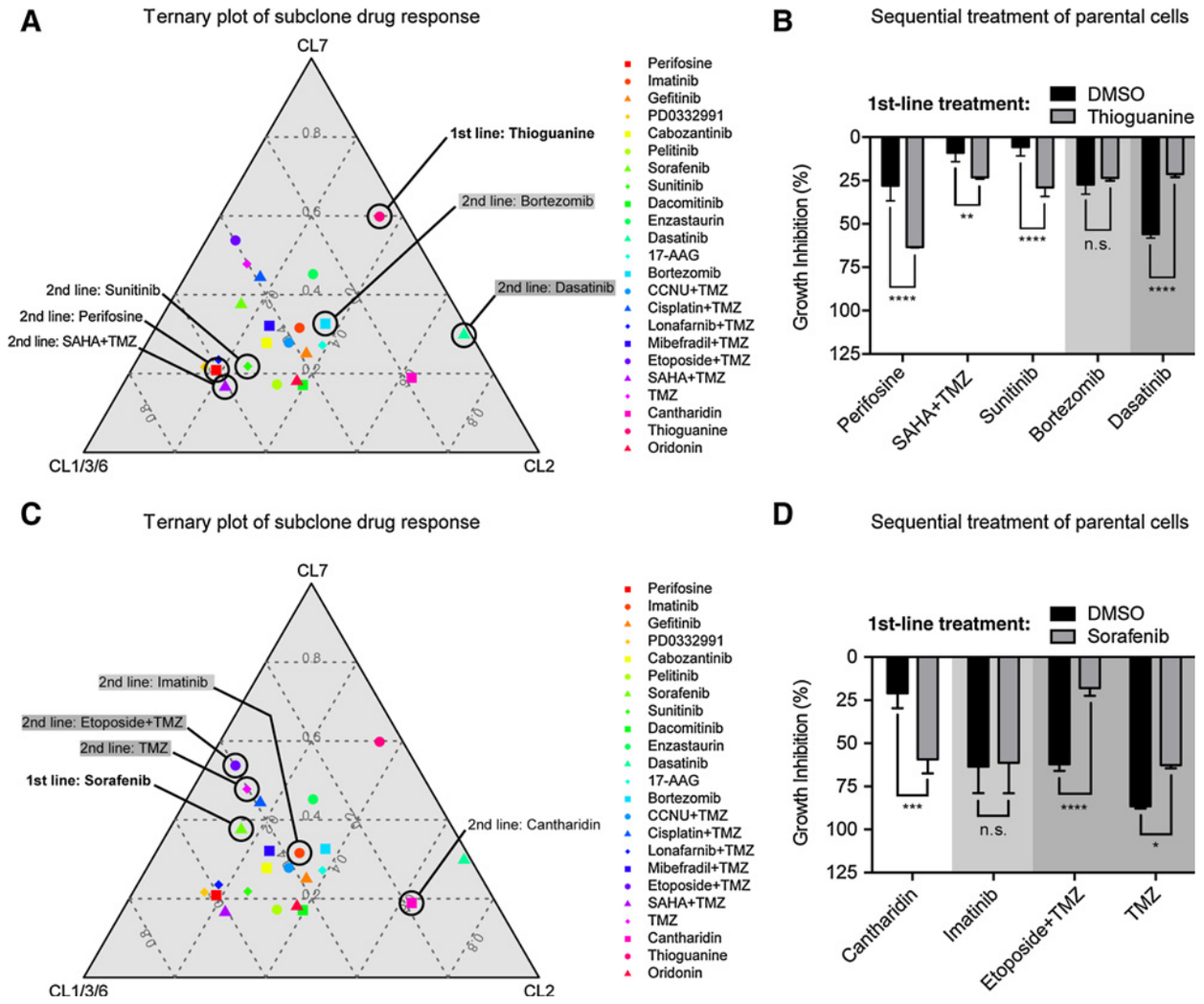

Figure 6.

Implications of predictable population dynamics for second-line treatment strategies. **A,** Ternary plots visualize the pharmacologic profiling data of the three GNV019 hierarchies in a two-dimensional plot (IC_{50} values, average data for CL1/3/6; compare Fig. 1 and Fig 4C; Supplementary Fig. S1). Every data point represents the positioning of a tested drug in relation to the respective cellular hierarchies. A drug that plots in close proximity to an edge in the graph has a strong inhibitory effect on the respective hierarchy and little effects on the others. Increasing distance from a corner implies decreasing sensitivity of the drug toward the respective hierarchy. For the first-line setting of thioguanine-based enrichment of CL1/3/6-like cells, second-line drugs were chosen as indicated in the plot: sunitinib, perifosine, and SAHA + temozolomide (TMZ) plotted close to the CL1/3/6 hierarchy, thus predicted highly effective sequential partners. Bortezomib (light gray) and dasatinib (dark gray) were predicted less effective. **B,** Investigations on GNV019 parental cells: graph representing data from sequential application of thioguanine/DMSO, followed by the chosen drugs from **A**. Note the high consistency of predictions on effectiveness of second-line drug applications. **C,** For the first-line setting of sorafenib-based enrichment of CL2-like cells, second-line drugs were chosen as indicated in the plot: cantharidin plotted close to the CL2 hierarchy and thus predicted a highly effective sequential partner. Imatinib (light gray) and temozolomide/etoposide + temozolomide (dark gray) were predicted less effective. **D,** Investigations on GNV019 parental cells: graph representing data from sequential application of sorafenib/DMSO, followed by the chosen drugs from **C**. Note the high consistency of predictions on effectiveness of second-line drug applications. Experiments were performed in triplicates. Significance levels: *, $P < 0.05$; **, $P < 0.01$; ***, $P < 0.001$; ****, $P < 0.0001$. n.s., not significant. CCNU, chloroethy-cyclohexyl-nitroso-urea (lomustine).

patients, we here show the applicability of discriminative *ex vivo* drug profiling of subclones from clinical samples. A previously unrecognized feasibility is revealed, enabling predictions on intratumoral drug response and the resulting population shifts in bulk tumor samples. This note has important implications, particularly in light of the additional finding that pharmacologic profiles could serve as a valuable asset for defining appropriate drug combinations for individualized sequential application.

The roots of our work are classic cell culture studies describing intratumoral diversity of karyotypes, phenotypes, and pharmacologic responses in human glioma (30–32), recently revisited by investigating patterns of receptor tyrosine kinase amplifications and their respective functional dependence *in vitro* (33). Taking advantage of stem/precursor culture conditions that enable maintenance of phenotypic and genetic properties, we demonstrate that isolated subclones are amenable for profiling and for

predictions on drug-related intratumoral dynamics. The importance of investigating alterations to the cellular composition of solid cancers before and after treatment is being increasingly revealed (e.g., refs. 34, 35). Drug-related enrichments of primary resistant cell types may even include minority cellular hierarchies of the original tumor (36, 37). This could be recapitulated in our model by the significant drug-related enrichment of CL1/3/6-like or CL2-like GNV019 hierarchies. We observed the effect even occurring independent of a survival benefit in xenografts. A logical next step for future follow-up would be a study on matched clinical samples obtained before and after treatment to provide unequivocal evidence that predictable drug-related clonal selection occurs in glioblastoma patients. We already know that successful eradication of targeted neoplastic cells cannot prevent the cells that were not targeted to develop fatal relapse (e.g., ref. 38). Predictable population dynamics could serve as a valuable asset on these grounds for defining appropriate secondary lines of treatment. It might even be essential, because secondary surgery cannot always be performed in glioblastoma, and current practice of care frequently considers rechallenge of first-line pharmacotherapy for treating relapsed disease (39).

It needs to be emphasized, however, that our approach focused on the feature of primary/intrinsic resistance. Further investigation may be directed, for example, toward acquired drug resistance and potential subclone interactions, as well as toward environmental and immunologic cues for a more comprehensive view (12, 40–42). Some of these factors, in addition to animal model–inherent obstacles, including potentially suboptimal drug dosage/pharmacokinetics/distribution, might already explain the lower efficacy of *in vivo* versus *in vitro* subclone enrichment observed in our study. Another restriction may apply to conditions for derivation and expansion of clinical samples. Although our work shows how cellular heterogeneity can be captured and how cellular identity can remain stable under adherent conditions, it is known that any setting of primary cell culture may inflict selection bias on patient tissue and cells (e.g., ref. 43). Thus, even though we present data on drug-mediated enrichment of 19 subclones from three clinical specimens, sufficient data are not available for a statistically valid extrapolation of clonal diversity. This could be addressed in future, for example, by introducing artificial DNA barcodes to the entire population, facilitating quantification of individual subclones in the tumor bulk (44).

Our study furthermore provides tools for individualizing medicine, for example, specifying how subclone drug profiles could help to foster translational studies and more personalized approaches addressing the functional consequences of intratumor heterogeneity (see Supplementary Fig. S8). In our study, ternary plots serve as schematic representations of subclone drug profiles. They correlate the degree of drug sensitivity among coexisting tumor cell hierarchies in a two-dimensional plot. Applied as a planning tool, suited pairs of drugs can be identified that drive the heterogeneous parental tumor bulk toward enrichment of a particular subclone/hierarchy during first-line application and that aim for depletion of this hierarchy in the second-line approach. Granted that future developments in clinical medicine will improve upon many of the technical aspects of our work, for example, toward a more complete mirroring of subclone heterogeneity from clinical specimens, our approach could provide the rationale for personalizing sequential therapy in glioblastoma. For basic sciences, the approach could enable investigation of potential relationships between drug-specific mechanisms of actions, differential drug sensitivities, and the various molecular signatures provided by intratumor hierarchies. Also, preclinical limitations, for example, inflicted by combinatorial versus sequential drug application, could be studied in a reductionist setting.

Taken together, our observations support accumulating evidence from the study of many malignant types of cancer and the notion that population-level methods could underestimate clinically relevant information (3–5, 14, 36, 45). Pharmacologic predictions on tumor dynamics would smoothly integrate into the intense ongoing search for new and alternative pharmacotherapy options, particularly needed in the setting of defining individualized second-line treatment strategies. Combined with advanced genetic diagnostics and driven by the high medical need in glioblastoma, this strategy might become an essential tool for precision medicine and clinical trial design (9).

Disclosure of Potential Conflicts of Interest

O. Brüstle has ownership interest (including patents) in LIFE & BRAIN GmbH, D.A. Steindler has ownership interest (including patents) in Prana Tx. B. Scheffler has conducted contract-based research for LIFE & BRAIN GmbH. No potential conflicts of interest were disclosed by the other authors.

Authors' Contributions

Conception and design: R. Reinartz, M. Glas, B.A. Reynolds, D.A. Steindler, B. Scheffler

Development of methodology: R. Reinartz, S. Wang, D.J. Silver, A. Wieland, T.M. Shepherd, M. Glas, Y. Liu, M. Simon, D.A. Steindler, B. Scheffler

Acquisition of data (provided animals, acquired and managed patients, provided facilities, etc.): R. Reinartz, S. Wang, S. Kebir, D.J. Silver, A. Wieland, T. Zheng, T.M. Shepherd, N. Schäfer, M. Glas, A.M. Hillmer, S. Cichon, A.A. Smith, T. Pietsch, A. Yachnis, M. Simon, D.A. Steindler, B. Scheffler

Analysis and interpretation of data (e.g., statistical analysis, biostatistics, computational analysis): R. Reinartz, S. Wang, S. Kebir, D.J. Silver, M. Küpper, L. Rauschenbach, R. Fimmers, T.M. Shepherd, N. Schäfer, M. Glas, A.M. Hillmer, S. Cichon, T. Pietsch, Y. Liu, O. Brüstle, D.A. Steindler, B. Scheffler

Writing, review, and/or revision of the manuscript: R. Reinartz, S. Kebir, D.J. Silver, T. Zheng, L. Rauschenbach, T.M. Shepherd, D. Trageser, A. Till, N. Schäfer, M. Glas, A.M. Hillmer, S. Cichon, A.A. Smith, T. Pietsch, Y. Liu, B.A. Reynolds, A. Yachnis, D.W. Pincus, M. Simon, O. Brüstle, D.A. Steindler, B. Scheffler

Administrative, technical, or material support (i.e., reporting or organizing data, constructing databases): S. Kebir, M. Glas, T. Pietsch, M. Simon, O. Brüstle, B. Scheffler

Study supervision: D.A. Steindler, B. Scheffler

Acknowledgments

We would like to thank Heike Höfer, Mihaela Keller, Anke Leinhaas, Sabine Normann, and Ramona Schelle for technical assistance, Dr. Philipp Koch for providing study material, Stefan Herms and the group of Dr. J. Schultze (LIMES-Institute, University of Bonn) for help with bioinformatics in this study. The authors thank the Departments of Neurosurgery and Neuropathology at the University of Bonn Medical Center for their assistance in tumor procurement and for the processing of paraffin-embedded samples. We thank Robert Schuit and Suvi Savola (MRC Holland) for providing P345-X1 & P346-X custom MLPA kits.

Grant Support

This study was mainly supported by the Lichtenberg program of the VW foundation (to B. Scheffler); additional funds were provided by the Federal Ministry of Education and Research, Germany (B. Scheffler/M. Glas; BMBF, VIP

initiative, FKZ 03V0785), and NIH/NINDS grant NS055165 (to D.A. Steindler). O. Brüstle support included EU FP7-HEALTH-2010-266753-SCR&Tox, COLIPA, BIO.NRW z0911bt027i, StemCellFactory, and Hertie Foundation.

The costs of publication of this article were defrayed in part by the payment of page charges. This article must therefore be hereby marked *advertisement* in accordance with 18 U.S.C. Section 1734 solely to indicate this fact.

Received September 11, 2015; revised June 13, 2016; accepted July 4, 2016; published OnlineFirst August 12, 2016.

References

1. Nowell PC. The clonal evolution of tumor cell populations. Science 1976;194:23–8.
2. Hanahan D, Weinberg RA. Hallmarks of cancer: the next generation. Cell 2011;144:646–74.
3. Navin N, Kendall J, Troge J, Andrews P, Rodgers L, McIndoo J, et al. Tumour evolution inferred by single-cell sequencing. Nature 2011; 472:90–4.
4. Snuderl M, Fazlollahi L, Le LP, Nitta M, Zhelyazkova BH, Davidson CJ, et al. Mosaic amplification of multiple receptor tyrosine kinase genes in glioblastoma. Cancer Cell 2011;20:810–7.
5. Gerlinger M, Rowan AJ, Horswell S, Larkin J, Endesfelder D, Gronroos E, et al. Intratumor heterogeneity and branched evolution revealed by multiregion sequencing. N Engl J Med 2012;366: 883–92.
6. Maley CC, Galipeau PC, Finley JC, Wongsurawat VJ, Li X, Sanchez CA, et al. Genetic clonal diversity predicts progression to esophageal adenocarcinoma. Nat Genet 2006;38:468–73.
7. Yap TA, Gerlinger M, Futreal PA, Pusztai L, Swanton C. Intratumor heterogeneity: seeing the wood for the trees. Sci Transl Med 2012;4: 127ps10.
8. Mroz EA, Tward AD, Pickering CR, Myers JN, Ferris RL, Rocco JW. High intratumor genetic heterogeneity is related to worse outcome in patients with head and neck squamous cell carcinoma. Cancer 2013;119:3034–42.
9. Bedard PL, Hansen AR, Ratain MJ, Siu LL. Tumour heterogeneity in the clinic. Nature 2013;501:355–64.
10. Ashworth A, Lord CJ, Reis-Filho JS. Genetic interactions in cancer progression and treatment. Cell 2011;145:30–8.
11. Westphal M, Lamszus K. The neurobiology of gliomas: from cell biology to the development of therapeutic approaches. Nat Rev Neurosci 2011;12: 495–508.
12. Valent P, Bonnet D, De Maria R, Lapidot T, Copland M, Melo JV, et al. Cancer stem cell definitions and terminology: the devil is in the details. Nat Rev Cancer 2012;12:767–75.
13. Meacham CE, Morrison SJ. Tumour heterogeneity and cancer cell plasticity. Nature 2013;501:328–37.
14. Meyer M, Reimand J, Lan X, Head R, Zhu X, Kushida M, et al. Single cell-derived clonal analysis of human glioblastoma links functional and genomic heterogeneity. Proc Natl Acad Sci U S A 2015;112:851–6.
15. Louis DN, Ohgaki H, Wiestler OD, Cavenee WK, Burger PC, Jouvet A, et al. The 2007 WHO classification of tumours of the central nervous system. Acta Neuropathol 2007;114:97–109.
16. Louis DN, Ohgaki H, Wiestler OD, Cavenee WK. WHO classification of tumours of the central nervous system. Geneva: World Health Organization; 2007.
17. Glas M, Rath BH, Simon M, Reinartz R, Schramme A, Trageser D, et al. Residual tumor cells are unique cellular targets in glioblastoma. Ann Neurol 2010;68:264–9.
18. Wieland A, Trageser D, Gogolok S, Reinartz R, Hofer H, Keller M, et al. Anticancer effects of niclosamide in human glioblastoma. Clin Cancer Res 2013;19:4124–36.
19. Koch P, Opitz T, Steinbeck JA, Ladewig J, Brustle O. A rosette-type, self-renewing human ES cell-derived neural stem cell with potential for in vitro instruction and synaptic integration. Proc Natl Acad Sci U S A 2009; 106:3225–30.
20. Scheffler B, Walton NM, Lin DD, Goetz AK, Enikolopov G, Roper SN, et al. Phenotypic and functional characterization of adult brain neuropoiesis. Proc Natl Acad Sci U S A 2005;102:9353–8.
21. Adams DH, Bowman BM. The chemotherapy of established sarcoma 180 and adenocarcinoma 755 tumors with 6-Thioguanine. Cancer Res 1963;23:883–9.
22. Siegelin MD, Raskett CM, Gilbert CA, Ross AH, Altieri DC. Sorafenib exerts anti-glioma activity *in vitro* and *in vivo*. Neurosci Lett 2010; 478:165–70.
23. R Core Team. R: a language and environment for statistical computing. Vienna: R Foundation for Statistical Computing; 2013.
24. Verhaak RG, Hoadley KA, Purdom E, Wang V, Qi Y, Wilkerson MD, et al. Integrated genomic analysis identifies clinically relevant subtypes of glioblastoma characterized by abnormalities in PDGFRA, IDH1, EGFR, and NF1. Cancer Cell 2010;17:98–110.
25. Patel AP, Tirosh I, Trombetta JJ, Shalek AK, Gillespie SM, Wakimoto H, et al. Single-cell RNA-seq highlights intratumoral heterogeneity in primary glioblastoma. Science 2014;344:1396–401.
26. Hegi ME, Diserens AC, Gorlia T, Hamou MF, de Tribolet N, Weller M, et al. MGMT gene silencing and benefit from temozolomide in glioblastoma. N Engl J Med 2005;352:997–1003.
27. Pollard SM, Yoshikawa K, Clarke ID, Danovi D, Stricker S, Russell R, et al. Glioma stem cell lines expanded in adherent culture have tumor-specific phenotypes and are suitable for chemical and genetic screens. Cell Stem Cell 2009;4:568–80.
28. Beroukhim R, Getz G, Nghiemphu L, Barretina J, Hsueh T, Linhart D, et al. Assessing the significance of chromosomal aberrations in cancer: methodology and application to glioma. Proc Natl Acad Sci U S A 2007;104: 20007–12.
29. The Cancer Genome Atlas Research Network. Comprehensive genomic characterization defines human glioblastoma genes and core pathways. Nature 2008;455:1061–8.
30. Shapiro JR, Yung WK, Shapiro WR. Isolation, karyotype, and clonal growth of heterogeneous subpopulations of human malignant gliomas. Cancer Res 1981;41:2349–59.
31. Wikstrand CJ, Bigner SH, Bigner DD. Demonstration of complex antigenic heterogeneity in a human glioma cell line and eight derived clones by specific monoclonal antibodies. Cancer Res 1983; 43:3327–34.
32. Yung WK, Shapiro JR, Shapiro WR. Heterogeneous chemosensitivities of subpopulations of human glioma cells in culture. Cancer Res 1982; 42:992–8.
33. Szerlip NJ, Pedraza A, Chakravarty D, Azim M, McGuire J, Fang Y, et al. Intratumoral heterogeneity of receptor tyrosine kinases EGFR and PDGFRA amplification in glioblastoma defines subpopulations with distinct growth factor response. Proc Natl Acad Sci U S A 2012; 109:3041–6.
34. Almendro V, Cheng YK, Randles A, Itzkovitz S, Marusyk A, Ametller E, et al. Inference of tumor evolution during chemotherapy by computational modeling and in situ analysis of genetic and phenotypic cellular diversity. Cell Rep 2014;6:514–27.
35. Kim J, Lee IH, Cho HJ, Park CK, Jung YS, Kim Y, et al. Spatiotemporal evolution of the primary glioblastoma genome. Cancer Cell. 2015;28: 318–28.
36. Diaz LAJr, Williams RT, Wu J, Kinde I, Hecht JR, Berlin J, et al. The molecular evolution of acquired resistance to targeted EGFR blockade in colorectal cancers. Nature 2012;486:537–40.
37. Kreso A, O'Brien CA, van Galen P, Gan OI, Notta F, Brown AM, et al. Variable clonal repopulation dynamics influence chemotherapy response in colorectal cancer. Science 2013;339:543–8.
38. Sampson JH, Heimberger AB, Archer GE, Aldape KD, Friedman AH, Friedman HS, et al. Immunologic escape after prolonged progression-free survival with epidermal growth factor receptor variant III peptide vaccination in patients with newly diagnosed glioblastoma. J Clin Oncol 2010;28:4722–9.
39. Weller M, Cloughesy T, Perry JR, Wick W. Standards of care for treatment of recurrent glioblastoma–are we there yet? Neuro Oncol 2013;15:4–27.

40. Marusyk A, Almendro V, Polyak K. Intra-tumour heterogeneity: a looking glass for cancer? Nat Rev Cancer 2012;12:323–34.
41. Vermeulen L, de Sousa e Melo F, Richel DJ, Medema JP. The developing cancer stem-cell model: clinical challenges and opportunities. Lancet Oncol 2012;13:e83–9.
42. Cloughesy TF, Cavenee WK, Mischel PS. Glioblastoma: from molecular pathology to targeted treatment. Annu Rev Pathol 2014; 9:1–25.
43. Reynolds BA, Vescovi AL. Brain cancer stem cells: think twice before going flat. Cell Stem Cell 2009;5:466–7.
44. Bhang HE, Ruddy DA, Krishnamurthy Radhakrishna V, Caushi JX, Zhao R, Hims MM, et al. Studying clonal dynamics in response to cancer therapy using high-complexity barcoding. Nat Med 2015;21:440–8.
45. Sottoriva A, Spiteri I, Piccirillo SG, Touloumis A, Collins VP, Marioni JC, et al. Intratumor heterogeneity in human glioblastoma reflects cancer evolutionary dynamics. Proc Natl Acad Sci U S A 2013;110:4009–14.